



Modeling the voltage nonlinearity of high-*k* MIM capacitors



D. Kannadassan^a, R. Karthik^a, Maryam Shojaei Baghini^b, P.S. Mallick^{a,*}

^a School of Electrical Engineering, VIT University, Vellore 632014, India

^b Department of Electrical Engineering, Indian Institute of Technology – Bombay, Powai, Mumbai 400076, India

ARTICLE INFO

Article history:

Received 7 June 2013

Received in revised form 11 October 2013

Accepted 12 October 2013

Available online 6 November 2013

The review of this paper was arranged by Prof. A. Zaslavsky

Keywords:

Voltage nonlinearity

High-*k* dielectrics

MIM capacitor

Ionic polarization

Induced dipoles

ABSTRACT

Voltage nonlinearity is a crucial performance parameter of MIM capacitors for RF, analog and mixed signal IC applications. In present work, the fabrication and characterization of anodic high-*k* MIM capacitors are reported in detail and modeling of nonlinearity coefficient of capacitance is developed using polarization of induced dipoles. The model agrees with experimental results for various high-*k* dielectric MIM capacitors. It explores the origin of nonlinearity in capacitance–voltage characteristics of MIM capacitors and also predicts the potential requirements to meet the ITRS requirements.

© 2013 Elsevier Ltd. All rights reserved.

1. Introduction

Analog and Mixed Signal (AMS) integrated circuits are employing metal–insulator–metal (MIM) capacitors for various sensitive applications, such as A/D converters, filters and phase shifters [1]. These circuits need MIM capacitors with a low voltage nonlinearity coefficient which measures the dependency of capacitance with applied voltage. According to International Technology Roadmap for Semiconductor (ITRS) [2], MIM capacitors should hold voltage nonlinearity coefficient of $<100 \text{ ppm/V}^2$ for AMS applications. High capacitance density of $>5 \text{ fF}/\mu\text{m}^2$ and low leakage current density of $<10^{-8} \text{ A/cm}^2$ are another two major challenges in MIM capacitors. Many authors have reported the fabrication of MIM capacitors with various high-*k* dielectrics to meet these challenging limits [3–6].

Single high-*k* dielectric layer MIM capacitor with voltage nonlinearity coefficient of $<= 100 \text{ ppm/V}^2$ is rarely achieved. This is due to the strong dependence of linearity coefficient with dielectric constant [7]. Wenger et al. experimentally proved that quadratic coefficient α increases as dielectric constant increases [7]. But the origin of the voltage nonlinearity is not clear. Some authors attempted to model the voltage nonlinearity using orientation polarization [8], electrode polarization [9], electrostriction [7] and ionic polarization [10]. However, most of them are either complex or

biased to particular materials. In this report, we present a generalized model of voltage nonlinearity for MIM capacitors using microscopic and macroscopic ionic polarizations. The model was verified with measured data of fabricated MIM capacitors.

Recently, many authors have reported fabrication of high-*k* dielectric MIM capacitors using anodization [11–13]. Anodization or anodic oxidation is an electrochemical method which yields crystalline high-*k* dielectrics with low structural defects and improved polarization properties [14]. Polarization processes involving in formation of capacitance for barrier type anodic oxides was reported by Kosjuk et al. [15]. It is concluded that deformation and ionic polarizations are dominant in anodic oxides of Al, Ta and Nb. It is also reported that anodic alumina shows a less sensitivity of capacitance with frequency compared to anodic Ta₂O₅ and Nb₂O₅ [15]. In this report, we have presented the fabrication of barrier type Al₂O₃ and TiO₂ MIM capacitors using anodic oxidation. The capacitance–voltage characteristics and crystalline properties are discussed. These modeling and experimental studies can map the dependable elements of voltage linearity, such as dielectric thickness and dielectric constant, which are required to meet the ITRS recommendations.

2. Fabrication

A 100 nm of SiO₂ thin film on Si substrate was grown using wet oxidation. Over that, an Al (99.99% pure) thin film of 300 nm was deposited by thermal deposition using tungsten filament at

* Corresponding author. Tel.: +91 416 220 2460; fax: +91 416 224 3092.

E-mail address: psmallick@vit.ac.in (P.S. Mallick).

pressure of 2.5×10^5 Torr. At 0°C , surrounded by ice bath, the Al film was anodized for anodization time T_A at constant anodization voltage of V_A in a solution of ammonium pentaborate (APB) dissolved in ethylene glycol (20 g l^{-1}) by platinum cathode of equal size as anode, in a constant current density of 0.5 mA/cm^2 . The solution was prepared by adding 17 g of APB for every 100 ml of ethylene glycol [16]. Etching for bottom electrode is avoided by dipping only three quarters of sample area in the electrolyte. Once cleaned thoroughly by deionized water, the 50 nm thick Al top electrode was deposited using thermal deposition with the shadow mask area of 0.6 mm^2 . Fig. 1(a) shows the schematic view of the fabricated MIM capacitors. SEM cross sectional view of anodization region of sample anodized at $V_A = 30\text{ V}$ for $T_A = 1\text{ min}$ is shown in Fig. 1(b). The surface profile of anodized region is shown in Fig. 1(c) which confirms ‘non-porous’ or ‘barrier type’ anodic Al_2O_3 . Fig. 1(d) shows the X-ray diffraction (XRD) spectra as a function of scattering angle (2θ) of the same sample. The crystalline peaks at 46.2° and 67.7° are observed which confirms that the formed oxide is $\gamma\text{-Al}_2\text{O}_3$.

The Al/TiO₂/Al (MIM) structure was fabricated in the following manner. A bilayer of Ti/Al (15 nm/100 nm) was deposited using electron-beam evaporator with tungsten filament over a 100 nm thermally oxidized silicon dioxide on silicon substrate. Here, Al acts as bottom electrode, which controls the thickness of TiO₂ during anodization. Ti film was potentiostatically anodized in APB using platinum cathode. Anodization was done for anodization voltages of 10 V, 15 V and 20 V till the current density reduced to 1 mA/cm^2 . To avoid etching of bottom electrode, only three

quarters of sample area was dipped in the electrolyte. 50 nm thick Al top electrode was deposited on the anodized samples after cleaned thoroughly by deionised water. Fig. 2(a) shows the SEM cross section of anodized sample at $V_A = 20\text{ V}$ before top electrode deposition and Fig. 2(b) shows the XRD spectra of respective sample. It was observed that the prepared TiO₂ at lower anodization voltage has crystalline phases of dominantly rutile with anatase and partially amorphous [17]. At higher anodization voltages, the amorphous state is transferred to crystalline/quasicrystalline state (anatase) with a thin interfacial layer of AlTiO (Alloy of both TiO₂ and Al₂O₃). The crystallization of anodic TiO₂ was reported in our earlier article [17].

3. Modeling of voltage nonlinearity

The thickness and dielectric constant of dielectric material have strong influence on voltage nonlinearity of MIM capacitors. We have developed a model to address this dependence of capacitance with applied voltage using macroscopic and microscopic polarization of high- k dielectrics.

3.1. Macroscopic model

The voltage dependent dielectric constant is a result of ionic polarization of induced dipoles and orientation polarization of permanent dipole for the applied field. The paraelectric material, such as Al₂O₃, TiO₂ and Ta₂O₃, are called non-polar oxides since

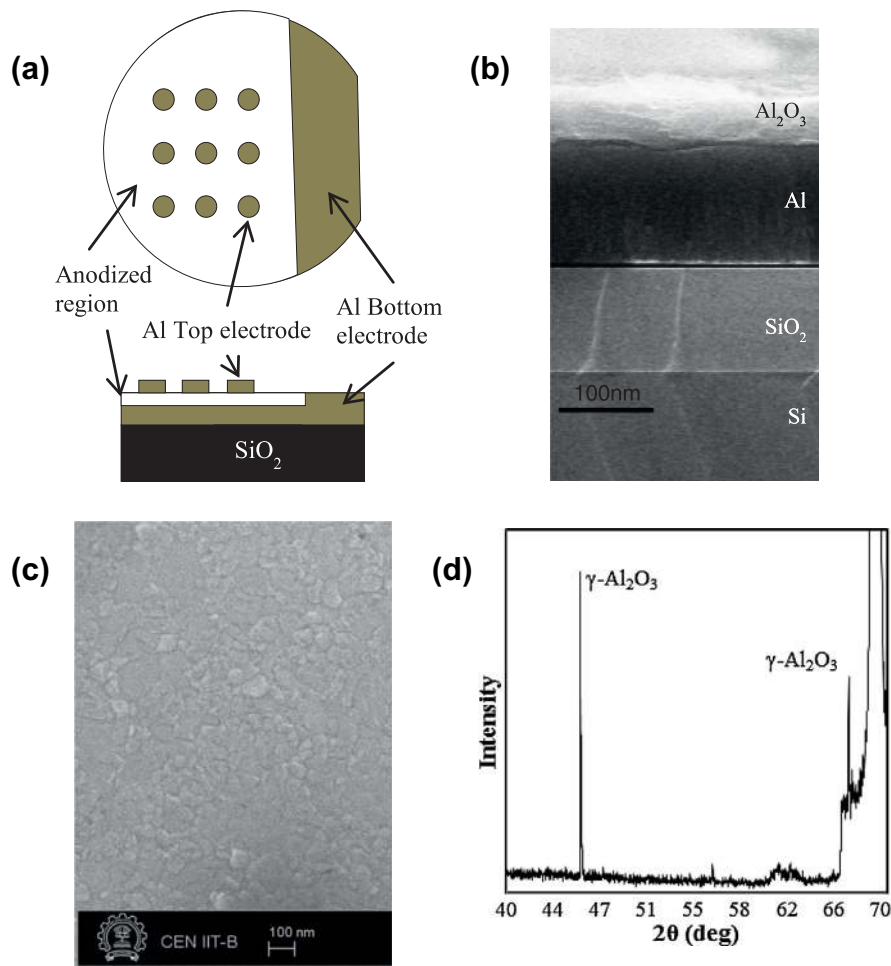


Fig. 1. (a) Schematic view of resulting MIM capacitors. (b) SEM cross sectional view of anodized Al_2O_3 sample at 30 V for 1 min at 0.5 mA/cm^2 , (c) surface and (d) XRD spectra.

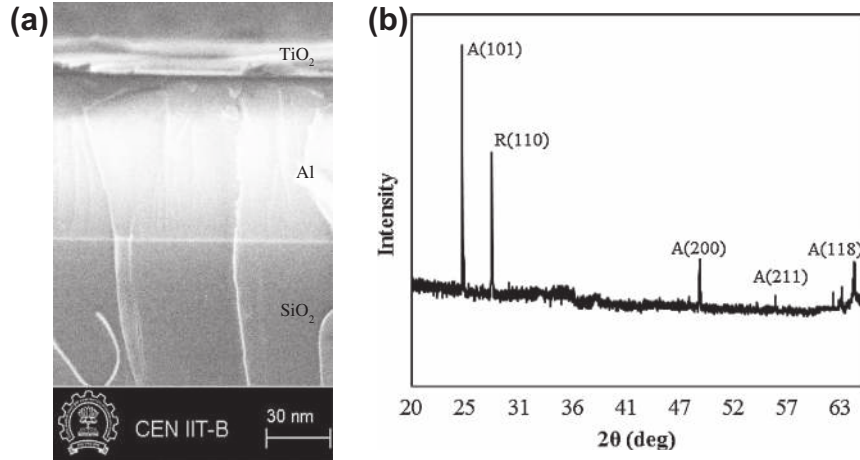


Fig. 2. (a) SEM cross sectional view of anodized TiO₂ sample at 20 V and (b) XRD spectra, A–Anatase and R–Rutile.

they do not have permanent dipoles. The metal–oxygen bond of these dielectric materials distorted by the applied field forms the induced dipole [18].

If angle between the induced dipole moment $\mu = \alpha_{ie}E$ and the applied electric field E is θ , then the average induced dipole moment can be expressed as $\bar{M} = \alpha_{ie}\overline{\cos^2\theta}E_{loc}$ [19]. Here α_{ie} is the internal electronic polarizability which is a microscopic quantity. E_{loc} is the local electric field within the dipole sphere which changes with respect to the position in dielectric layer from electrode. This is expressed as $E_{loc} = \lambda E$ where λ is field correction factor. In Onsager Model, the neighboring molecules are also affecting the polarization and the field correction factor was derived as $\lambda = 3\epsilon_r/[2\epsilon_r + 1]$ [19]. With Boltzmann statistics, the mean value of $\cos^2\theta$ is given as,

$$\overline{\cos^2\theta} = \frac{\int_0^\pi \exp\left(\frac{\alpha_{ie}\cos^2\theta E_{loc}}{kT}\right) \cos^2\theta \sin\theta d\theta}{\int_0^\pi \exp\left(\frac{\alpha_{ie}\cos^2\theta E_{loc}}{kT}\right) \sin\theta d\theta} \quad (1)$$

which can be reduced to 2nd order Langevin function [20], $\overline{\cos^2\theta} = L_2(\beta) = 1 - \frac{2}{\beta}L(\beta)$, where, $L(\beta) = \frac{e^\beta + e^{-\beta}}{e^\beta - e^{-\beta}} - \frac{1}{\beta} = \coth\beta - \frac{1}{\beta}$ is referred as Langevin function [8,20] and $\beta = \frac{\alpha_{ie}E_{loc}}{kT}$. Thus, the average dipole moment can be expressed as $\bar{M} = \alpha_{ie}L_2(\beta)E_{loc}$. The total orientation polarizability of induced dipoles is $\alpha_{oi} = N_{di}\frac{\bar{M}}{E}$. Therefore,

$$\alpha_{oi} = N_{di}\lambda\alpha_{ie}L_2(\beta) \quad (2)$$

where $N_{di} = n_{di}Ad$ is the number of induced dipoles in dielectric layer for the uniform applied electric field, n_{di} is the density of induced dipoles per cubic volume, A and d are area and thickness of dielectric layer, respectively.

3.2. Microscopic model

The molecular electronic orientation is influenced by associated internal field within dipole and the external field. In Lorentz approach, the dipoles are modeled as sphere with few molecule/atoms inside [18] where the total internal electric field for isotropic materials is $E_{total} = E + E_{pol}$. E_{pol} is the field due to polarized charge distribution, expressed as $E_{pol} = \frac{P}{3\epsilon_0}$ with polarization P . The total internal electronic polarization per dipole is expressed as, $P_{ie} = \epsilon_0 N_{di}\alpha_{ie}(E + \frac{P}{3\epsilon_0})$ which can be rearranged as $P_{ie} = \frac{\epsilon_0 N_{di}\alpha_{ie}E}{1 - \frac{N_{di}\alpha_{ie}}{3}}$ [18]. α_{ie} is internal/induced electronic polarizability of charges within the dipole sphere. Since $P = \epsilon_0(\epsilon_r - 1)E = \epsilon_0\chi_e E$, this equation can be written as,

$$\alpha_{ie} = \frac{3\epsilon_0}{N_{di}} \left(\frac{\epsilon_r - 1}{\epsilon_r + 2} \right) \quad (3)$$

This is referred as Clausius–Mossotti equation. This equation relates the macroscopic element ϵ_r with microscopic element α_{ie} . Using these microscopic and macroscopic models of ionic polarization, the total polarization can be expressed as,

$$P = \left(\epsilon_0\chi_e + N_{di} \left[\frac{3\epsilon_0}{N_{di}} \left(\frac{\epsilon_r - 1}{\epsilon_r + 2} \right) \right] L_2(\beta) \right) E \quad (4)$$

The second order Langevin function can be approximated $L_2(E) \approx \frac{\beta^2}{15}$ for $\beta \ll 1$ or $\lambda\mu E \ll kT$ [20]. Therefore, the field dependent permittivity of dielectric layer can be expressed in term of static permittivity ϵ_r as,

$$\epsilon(V) = \epsilon_0 + \epsilon_0\chi_e + N_{di} \left[\frac{3\lambda\epsilon_0}{N_{di}} \left(\frac{\epsilon_r - 1}{\epsilon_r + 2} \right) \right]^3 \frac{E^2}{15(kT)^2} \quad (5)$$

This equation can be compared with the empirical relation, $C(V) = C_0(\alpha V^2 + \beta V + 1)$, where C_0 is the capacitance at bias voltage of zero. Therefore, the quadratic (α) coefficient of capacitance is,

$$\alpha \approx 1.8 \left(\frac{\epsilon_0}{N_{di}kT} \right)^2 \left[\lambda \left(\frac{\epsilon_r - 1}{\epsilon_r + 2} \right) \right]^3 \frac{1}{d^2} \quad (6)$$

The model shows that the α is inversely proportional to square of the thickness which shows a good agreement with the models proposed by Wenger et al. and Phung et al. [8,7]. It also shows that a has strong dependence with ϵ_r , which indicates that higher dielectric constant materials shall lead to large α . Eq. (6) shows that the α is inversely proportional to temperature, but it is observed that the α shows a linear relation with temperature T in many recent works [7,21]. This is due to increase in induced dipole moment with temperature which can be introduced as $\bar{M}(T) = \bar{M}\eta T$, where η is the increment factor of linear relation for the temperature T . This yield,

$$\alpha \approx 1.8 \left(\frac{\epsilon_0}{N_{di}k} \right)^2 \left[\eta \lambda \left(\frac{\epsilon_r - 1}{\epsilon_r + 2} \right) \right]^3 \frac{T}{d^2} \quad (7)$$

The polarization due to permanent dipoles of paraelectric materials can be modeled in accordance with [8]. Therefore, we can introduce the orientation polarization $P_o = N_{pd}\mu_{pd}L(\beta)$ in Eq. (4) as described in [8] where N_{pd} is the number of permanent dipoles and μ_{pd} is the dipole moment. It is observed that $L(\beta)$ converges to unity much

faster than $L_2(\beta)$ [20] which indicates that polar dielectric materials shall show a high α than that of paraelectrics.

4. Results and discussion

The fabrication of anodic Al_2O_3 and anodic TiO_2 MIM capacitors is explained in Section 2. The capacitance–voltage ($C-V$) characteristics were measured using HP4155C semiconductor parameter analyzer. Fig. 3(a) shows measured $C-V$ characteristics of Al_2O_3 MIM capacitors of various dielectric thicknesses. The voltage coefficient of capacitance (VCC) is extracted using $VCC = (C(V) - C_0)/C_0$ and is shown in Fig. 3(b), where C_0 is capacitance at zero bias. It is observed that the stability of capacitance is improved at higher thickness. This is due to reduction of local field in the bulk dielectrics and improved ionic polarization of anodic alumina. Obtained dielectric thickness of Al_2O_3 and measured capacitance density at applied bias voltages 2 V and 5 V as a function of V_A are shown in Fig. 4. A clear linear relation is observed between oxide thickness and anodization voltage with growth rate of 1.41 nm/v. Fig. 5 shows the measured $C-V$ characteristics of TiO_2 MIM Capacitors at room temperature. It shows that the capacitance is increased about $2fF/\mu m^2$ for higher anodization voltage which is due to improved crystalline property. Thin $AlTiO$ layer acts as interfacial layer between TiO_2 and Al bottom electrode. This helps in formation of capacitance and reduction of leakage current [17].

Quadratic coefficient of capacitance α is extracted from measured $C-V$ characteristics using empirical relation $C(V) = C_0(\alpha V^2 + \beta V + 1)$. The modeled and extracted α for both TiO_2 and Al_2O_3 MIM capacitors at room temperature ($\eta = 1$) are plotted as a function of dielectric thickness and is shown in Fig. 6. Measured α values of HfO_2 and Y_2O_3 MIM capacitors for various thicknesses are available in [7], which are also included in Fig. 6 to validate the model. Fitting parameters of the model for all materials are presented in Table 1. Al_2O_3 shows low α and good agreement with model. The crystalline state and strong ionic bond of anodic Al_2O_3 also support in reduction of α . It is observed that for the anodic TiO_2 capacitor, with same thickness of ~ 15 nm, the α decreases for higher anodization voltages which is due to transformation of amorphous to crystalline state and formation of thin $AlTiO$ interfacial layer. The migration of Al ions into TiO_2 layer reduces the effective thickness of TiO_2 which supports improvement of the capacitance. At the same time, these Al ions reduce the local field in the bulk TiO_2 . Since the Al ion distribution is not uniform and not dominant in TiO_2 layer, the interfacial layer is not considered as second layer. It is worth to note that a second layer of Al_2O_3 is formed at higher anodization of >20 V which was reported in our earlier work [22]. HfO_2 and Y_2O_3 MIM capacitors show a good fit with our model as shown in Fig. 6. Fitting compatibility of model with measured quadratic coefficient of capacitance

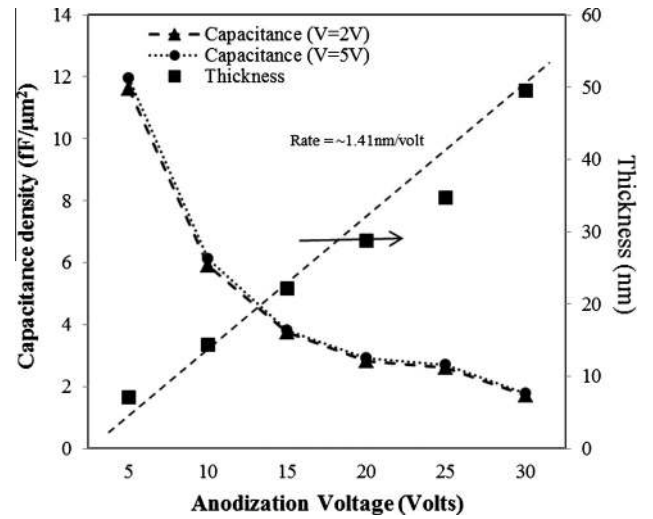


Fig. 4. Measured capacitance density and dielectric thickness of Al_2O_3 MIM capacitor.

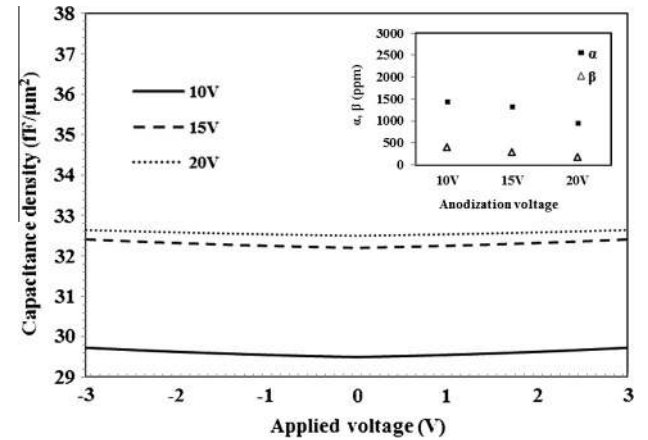


Fig. 5. Measured $C-V$ characteristics of all TiO_2 MIM capacitors.

at various temperatures is shown in Fig. 7. It is observed that titania MIM capacitor shows a strong dependence with temperature. This is due to weak ionic bond which leads to large distortion of metal–oxygen bond. MIM capacitors with alumina show a low dependence with temperature as thickness increases. It is due to decrease in field as thickness increases which in turn reduces the local field. Also it shows that the ionic bond of Al_2O_3 is strong and less sensitive to temperature.

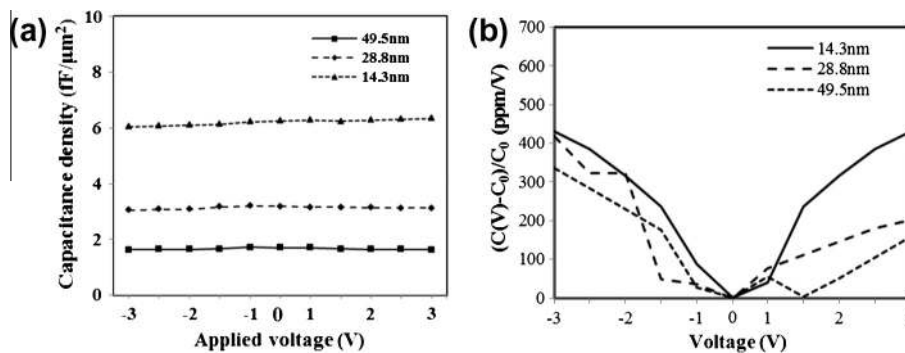


Fig. 3. (a) Measured $C-V$ characteristics of Al_2O_3 MIM capacitor for various thicknesses. (b) Extracted Voltage coefficient of capacitance.

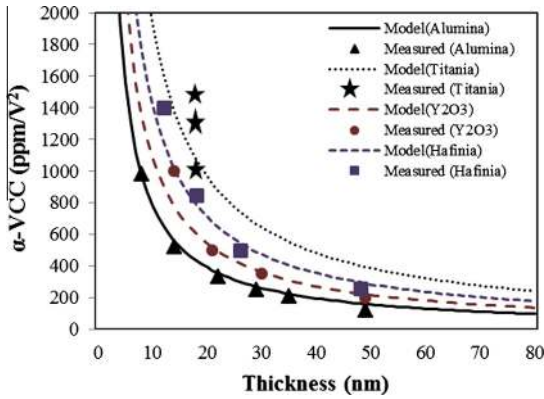


Fig. 6. Measured and modeled quadratic coefficient of capacitance α of various MIM capacitors.

Table 1
Material parameters for modeling.

Material	Al ₂ O ₃	TiO ₂	HfO ₂	Y ₂ O ₃
Dielectric constant (ϵ_r)	9	100	25	15
Induced dipole density (n_{di}) ($10^{22}/\text{cm}^3$)	6	10	4	4
Field correction factor (λ)	1.4210	1.4925	1.4516	1.4706

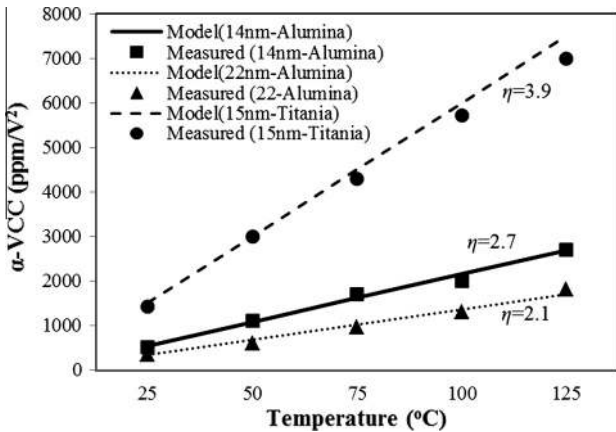


Fig. 7. Measured and modeled quadratic coefficient of capacitance α of various temperatures.

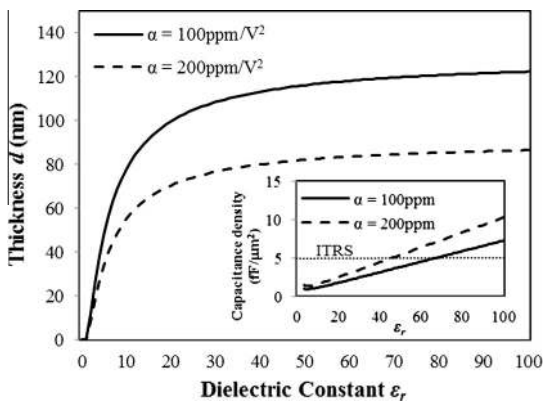


Fig. 8. Required thickness of dielectric to meet the ITRS recommendations for various dielectric constants. Inset: Maximum achievable capacitance density for the extracted thickness for $\alpha = 100 \text{ ppm/V}^2$ and $\alpha = 200 \text{ ppm/V}^2$.

The model can be used to explore the limitation of thickness and dielectric constant to meet the ITRS requirement. Fig. 8 shows the required physical thickness of dielectric layer to meet $\alpha = 100 \text{ ppm/V}^2$, assuming the average density of dipoles $n_{di} = 10 \times 10^{22} \text{ per cm}^3$. It is observed that required thickness d increases with dielectric constant ϵ_r . However, it saturates to $\sim 110 \text{ nm}$ after $\epsilon_r \sim 30$. This indicates that the high dielectric constant MIM capacitors require more than 100 nm thickness of dielectric layer to meet the ITRS recommendations. Fig. 8 also shows the required thickness if $\alpha = 200 \text{ ppm/V}^2$ is acceptable, which shows 20% reduction in thickness. Inset of Fig. 8 shows the maximum achievable capacitance density for the extracted thickness to meet $\alpha = 100 \text{ ppm/V}^2$ and $\alpha = 200 \text{ ppm/V}^2$. Fig. 8 and its inset are highly useful to select the material thickness and electrode area as per the IC design requirement. For vertical or thickness miniaturization, one should go for low dielectric material with higher electrode area to achieve high capacitance. For horizontal or area reduction of ICs, the thicker and higher dielectric constant layer is preferable. However, the technology limitations such as oxidation rate, deposition rate, defect density and ionic bonding of material play a major role in the performance of MIM capacitors. Inset of Fig. 8 shows that the MIM capacitors with high- k materials with dielectric constant of >60 will meet the ITRS recommendation in terms of capacitance density and voltage linearity. However, according to Mise et al. [23], materials with high dielectric constant of >60 show a very low effective barrier height at metal/insulator interface. This may lead to higher leakage current density of $>10^{-8} \text{ A/cm}^2$. A thin barrier layer of large bandgap material can be introduced along with high- k material to suppress the leakage current which intern reduces the voltage linearity.

5. Conclusion

Fabrication of crystalline Al₂O₃ and TiO₂ MIM capacitors using anodic oxidation is reported. The dependence of capacitance with voltage and thickness of these MIM capacitors is discussed in detail. The quadratic coefficient of capacitance, α , is modeled with microscopic and macroscopic ionic polarization of induced dipole. The model predicts that the origin of nonlinearity is the metal–oxygen bond distortion due to applied field. This distortion of ionic bond in dielectric molecule leads to such dependence of capacitance with applied voltage. This indicates the strong ionic bond between metal–oxygen which should be enhanced during fabrication process with some additional techniques, such as annealing or re-anodization. It predicts that the coefficient α is inversely proportional to square of dielectric thickness and directly proportional to dielectric constant. These observations have good agreement with experimental data of HfO₂, Y₂O₃, Al₂O₃ and TiO₂ MIM capacitors. The model can help to find the required thickness of high- k dielectric materials in MIM capacitors to meet the ITRS recommendations.

Acknowledgments

The authors would like to acknowledge financial support by Indian Nanoelectronics User’s Program (INUP), Government of India, through Center for Excellence in Nanoelectronics, IIT-Bombay. Authors also would like to thank Prof. A. Q. Contractor, Dr. K. Nageswari of IIT-Bombay, and Prof. Srinivasa Rao Zinka of VIT University for their support.

References

- [1] Ng CH, Ho CS, Chu SFS, Sun SC. MIM capacitor integration for mixed-signal/RF applications electron devices. *IEEE Transactions on* 2005;52:1399–409.
- [2] ITRS. International technology roadmap for semiconductor 2010. Report on RF and analog-mixed signal design; 2011.
- [3] Chen S, Lai C, Chin A, Hsieh J, Liu J. High-density MIM capacitors using Al₂O₃ and AlTiOx dielectrics. *Electron Dev Lett IEEE April* 2002;23:185–7.
- [4] Chiang KC, Lai CH, Chin A, Kao HL, McAlister SP, Chi CC. Very High Density RF MIM Capacitor Compatible with VLSI. *IEEE MTT-S Int Microw Sym Digest* 2005;2005:287–90.
- [5] Miao B, Mahapatra R, Jenkins R, Silvie J, Wright NG, Horsfall AB. Radiation induced change in defect density in HfO₂-based MIM capacitors. *IEEE Trans Nucl Sci* 2009;56(5):2916–24.
- [6] Perng T-H, Chien C-H, Chen C-W, Lehnen P, Chang C-Y. High-density MIM capacitors with HfO₂ dielectrics. *Thin Solid Films* 2004;469–470:345–9.
- [7] Wenger C, Lupina G, Lukosius M, Seifarth O, Mussig H, Pasko S, et al. Microscopic model for the nonlinear behavior of high-k metal–insulator–metal capacitors. *J Appl Phys* 2008;103(10).
- [8] Phung TH, Steinmann P, Wise R, Yeo Y, Zhu C. Modeling the negative quadratic VCC of SiO₂ in MIM capacitor. *IEEE Electron Device Lett* 2011;32(12):1671–3.
- [9] Gonon P, Vallae C. Modeling of nonlinearities in the capacitance–voltage characteristics of high-k metal–insulator–metal capacitors. *Appl Phys Lett* 2007;90(14).
- [10] Be'cu S, Cre'mer S, Autran J. Capacitance non-linearity study in Al₂O₃ MIM capacitors using an ionic polarization model. *Microelectron Eng* 2006;83(11–12):2422.
- [11] Hourdakis E, Nassiopoulou AG. High-density MIM capacitors with porous anodic alumina dielectric. *IEEE Trans Electron Devices* 2010;57(10):2679–83.
- [12] Hourdakis E, Nassiopoulou AG. High performance MIM capacitor using anodic alumina dielectric. *Microelectron Eng* 2012;90:12–4.
- [13] Sedghi N, Davey W, Mitrovic IZ, Hall S. Reliability studies on Ta₂O₅ high-kappa dielectric metal–insulator–metal capacitors prepared by wet anodization. *AVS* 2011;29. p. 01AB10.
- [14] Diggle JW, Downie TC, Goulding CW. Anodic oxide films on aluminum. *Chem Rev* 1969;69(3):365–405.
- [15] Kosjuk LM, Odynets LL. Polarization processes in anodic oxide films. *Thin Solid Films* 1997;302(1–2):235–8.
- [16] Kannadassan D, Karthik R, Bhagini M, Mallick P. Nanostructured barrier type anodic oxide metal–insulator–metal capacitors. *J Nanoelectronics and Optoelectronics* 2012;7(4):400–4.
- [17] Kannadassan D, Karthik R, Shojaei Baghini M, Mallick P. Nanostructured metal–insulator–metal capacitor with anodic titania. *Mater Sci Semicond Process* 2013;16(2):274–81.
- [18] Talebian E, Talebian M. A general review on the derivation of clausius–mossotti relation. *Optik* 2013;124(16):2324–6.
- [19] Neumann E. Chemical electric field effects in biological macromolecules. *Prog Biophys Mol Biol* 1986;47(3):197–231.
- [20] Gubin SP. *Magnetic nanoparticles*. John Wiley and Sons; 2009.
- [21] Kim SJ, Cho BJ, Li M, Ding S, Zhu C, Yu MB, et al. Improvement of voltage linearity in high-k MIM capacitors using HfO₂–SiO₂ stacked dielectric. *IEEE Electron Device Lett* 2004;25(8):538–40.
- [22] Karthik R, Kannadassan D, Shojaei Baghini Maryam, Mallick PS. Nanostructured bilayer anodic TiO₂/Al₂O₃ metal–insulator–metal capacitor. *J Nanosci Nanotechnol* 2013;13(10):6894–9.
- [23] Mise et al. Theoretical Screening of Candidate Materials for DRAM Capacitors and Experimental Demonstration of a Cubic-Hafnia MIM Capacitor. *IEEE Tran Elec. Dev.* 2010; Vol. 57(9): pp 2080.